ELSEVIER

Journal of Alloys and Compounds 404–406 (2005) 421–426

Journal of ALLOYS AND COMPOUNDS

www.elsevier.com/locate/jallcom

Vanadium-based BCC alloys: phase-structural characteristics and hydrogen sorption properties

M.V. Lototsky[a,b], V.A. Yartys[a,*], I.Yu. Zavaliy[c]

[a] *Institute for Energy Technology, P.O. Box 40, N-2027 Kjeller, Norway*
[b] *Institute for Problems of Materials Science of the National Academy of Sciences of Ukraine, 3, Krzhizhanovski Str., 03142 Kyiv, Ukraine*
[c] *Physico-Mechanical Institute of the National Academy of Sciences of Ukraine, 5, Naukova Str., Lviv 290601, Ukraine*

Received 16 August 2004; received in revised form 5 January 2005; accepted 11 January 2005
Available online 2 August 2005

Abstract

This work was focused on the studies of vanadium-based "low-temperature" bcc alloys as H storage materials. Both as cast and annealed at 1100 °C quaternary alloys $V_{92.5-x-y}Zr_{7.5}Ti_{7.5+x-y}M_y$ (M = Cr, Mn, Fe, Co, Ni; $x = 0$, 10; $y = 0$, 7.5) were studied. They were characterised by XRD, PCT hydrogen absorption–desorption measurements (T = 30–120 °C) and thermal desorption spectroscopy studies of H desorption from the saturated hydrides ($T = -100$ to 800 °C). The thermodynamics of the $VH_{\sim 2} \leftrightarrow VH_{\sim 1}$ transition and hydrogen sorption capacities (1.55, . . . , 1.80 H/M) were found to be significantly influenced by the substituting M-element. The reversible hydrogen storage capacity ($T < 100$ °C, $P > 0.1$ bar) reaches 50–60% of its overall value. Complete hydrogen desorption proceeds in vacuum at $T < 300$ °C. The major future challenge of the work is in increasing of the easy-reversible part of the H storage capacity corresponding to transformation $VH_{\sim 2} \leftrightarrow VH_{\sim 1}$ by reducing the content of H in the monohydride.

Keywords: Hydrogen storage materials; Gas–solid reactions; X-ray diffraction; Thermal analysis

1. Introduction

Vanadium dihydride (VH_2) has the highest known volumetric hydrogen storage capacity (0.16 g/cm^3 or 2.25 times more than the density of liquid hydrogen) and relatively high hydrogen weight capacity (3.78 wt.%). About 50% of this hydrogen is reversibly absorbed/desorbed at convenient conditions: at room temperature and pressures slightly higher than 1 bar. Residual hydrogen can be removed in vacuum at temperatures below 300 °C [1,2]. At the same time, the $VH_{\sim 2} \leftrightarrow VH_{\sim 1}$ transition is characterised by an incline temperature dependence of hydrogen equilibrium pressure, associated with unusually high values of entropy and enthalpy of the formation of the dihydride [3]. In addition, this transition has a strong inverse isotopic effect [4].

This unique combination of the properties of VH_2 opens broad possibilities for the thermally managed hydrogen storage applications. At the same time, practical use of VH_2 meets a number of difficulties. They include slow formation kinetics [5] and high sorption hysteresis [6]. Recently the growing efforts are focused to resolve these problems. In particular, doping of the vanadium–titanium alloys by small additives of transition elements (Cr, Mn, Ni and Zr) improves hydrogen sorption characteristics [5,7–10].

This work was aimed on studies of the phase-structural characteristics and hydrogen sorption properties of multi-component alloys having composition $V_{92.5-x-y}Zr_{7.5}Ti_{x+7.5-y}M_y$, where M = Cr, Mn, Fe, Co, Ni; $x = 0$, 10 and $y = 0$, 7.5. The selected ratio of the components was expected to provide the formation of the bcc solid solutions based on vanadium, being outside of the two-phase region where the formation of intermetallic phases takes place (Fig. 1).

2. Experimental

The alloys (∼3 g each) were prepared by argon arc melting. The starting materials had purity better than 99.9 wt.%.

* Corresponding author. Tel.: +47 63806453; fax: +47 63812905.
E-mail address: volodymyr.yartys@ife.no (V.A. Yartys).

0925-8388/$ – see front matter © 2005 Elsevier B.V. All rights reserved.
doi:10.1016/j.jallcom.2005.01.139

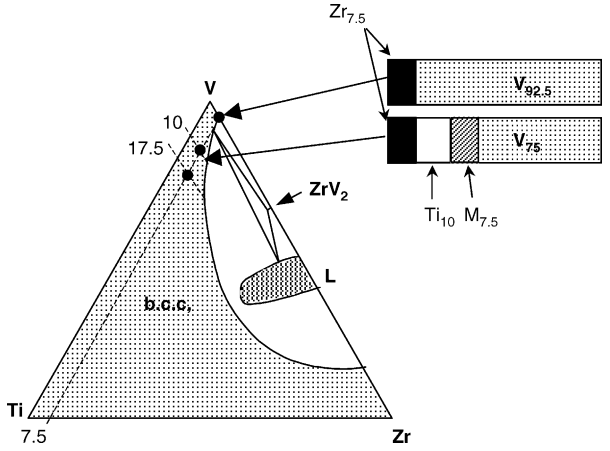

Fig. 1. Compositions of the studied alloys $V_{92.5-x-y}Zr_{7.5}Ti_{7.5+x-y}M_y$ (M = Cr, Mn, Fe, Co, Ni; $x = 0$, 10; $y = 0$, 7.5). Isothermal section of the phase diagram V–Ti–Zr at $T = 1300\,^{\circ}C$ [11] is given.

To improve their homogeneity, the ingots were remelted 2–3 times. The samples were annealed at $T = 1100\,^{\circ}C$ during 50 h, with a subsequent quenching into the mixture of ice and water.

Phase-structural characteristics of the samples (initial annealed alloy; "dihydride" obtained by H sorption at room temperature and ~20 bar pressure of H_2; "monohydride" obtained by H desorption from the "dihydride" at $T = 100\,^{\circ}C$ and $P < 0.01$ bar; and alloy after a completion of the desorption process obtained by heating of the hydride in vacuum to ~ 800 °C) were studied using XRD (Siemens D5000 diffractometer, Cu Kα_1 radiation, $2\theta = 10$–90°). The calculated X-ray patterns of the constituent phases were simulated using Powder Cell software and analysed in comparison with the reference structural data [12].

Hydrogen absorption/desorption characteristics were measured in the Sieverts-type setup. Further details can be found in [13]. Before the measurements, a bulk sample of the alloy (0.8–1.5 g) was activated by heating in vacuum to 450 °C during 1 h followed by a saturation with hydrogen gas. The activation was repeated until a complete reproducibility of the hydrogen sorption capacity was achieved.

The powdered sample ($m \sim 0.4$ g) was reloaded into the setup for the measurements of the PCT characteristics. These studies have been done in the pressure range 0.001–25 bar at temperatures from 30 to 120 °C. After measuring an absorption–desorption isotherm cycle, the sample was evacuated during 2 h at $T = 500\,^{\circ}C$ before the following series of the measurements at different temperature. The data were fitted using a recently developed PCT model [14].

The thermal desorption spectra of the hydrogen-saturated alloys were measured in the temperature range from −100 to 800 °C at a heating rate of 5°/min.

3. Results and discussion

3.1. Phase-structural characteristics

The annealed and as-cast samples have similar phase-structural characteristics containing β-phase solid solution as the main component. However, in addition small amounts of α-Zr are observed in the as-cast alloys which are converted on hydrogenation to ε-ZrH_x. α-Zr disappears after the annealing.

Summary of the results of the phase-structural characterisation of the annealed alloys and their corresponding hydrides is given in Table 1. Unit cell parameters of the main constituent, bcc solid solution, determined from X-ray studies of starting alloys, agree, within experimental error, with the data for the samples which underwent a hydrogenation–decomposition cycle.

All studied alloys contain, as a major constituent, the V-based bcc phase ($a = 3.03$ Å for pure V). The hydrogenation proceeds in two steps. The tetragonal "monohydride" V_2H_{1+x} (space group $I4_1/amd$; $a = 6.001$–6.035 Å, $c = 6.59$–6.87 Å) is formed first. Further absorption of hydrogen results in a formation of the fcc "dihydride" (space group $Fm\bar{3}m$, $a = 4.27$ Å for VH_2).

XRD patterns showed a formation of well-crystalline samples both for starting alloys and for dihydrides. However, only for the $V_{92.5}Zr_{7.5}$ sample a well-defined XRD pattern of the "monohydride" was observed. On the con-

Table 1
Crystallographic data of the annealed alloys and their hydrides

Designation[a]	Sample	Unit cell dimensions (Å)			Secondary phases
		Alloy	Monohydride	Dihydride	
(Ti)	$V_{75}Ti_{17.5}Zr_{7.5}$	3.040(1)	$a = 6.16(1)\,c = 6.65(1)$	4.295(1)	η[b]
(V)	$V_{92.5}Zr_{7.5}$	3.022(1)	$a = 6.067(3)\,c = 6.739(6)$	4.2712(9)	η, ZrO_2
(Cr)	$V_{75}Ti_{10}Zr_{7.5}Cr_{7.5}$	3.0349(7)	$a = 6.1932(3)\,c = 6.564(1)$	4.2830(4)	η, ZrO_2
(Mn)	$V_{75}Ti_{10}Zr_{7.5}Mn_{7.5}$	3.033(1)	$a = 6.07(2)\,c = 6.74(3)$	4.286(3)	η, C15[c]
(Fe)	$V_{75}Ti_{10}Zr_{7.5}Fe_{7.5}$	3.0283(9)	$a = 6.100(6)\,c = 6.76(1)$	4.263(1)	C14[d], η
(Co)	$V_{75}Ti_{10}Zr_{7.5}Co_{7.5}$	3.0357(5)	$a = 6.082(6)\,c = 6.73(1)$	4.263(2)	C14[d], η
(Ni)	$V_{75}Ti_{10}Zr_{7.5}Ni_{7.5}$	3.0248(4)	$a = 6.234(1)\,c = 6.580(9)$	4.255(1)	η

[a] The designations of the alloys presented in the first column are later used in the paper. Their compositions are shown in the second column.
[b] Structure type Fe_3W_3C, space group $Fd\bar{3}m$.
[c] Structure type $MgCu_2$, space group $Fd\bar{3}m$.
[d] Structure type $MgZn_2$, space group $P6_3/mmc$.

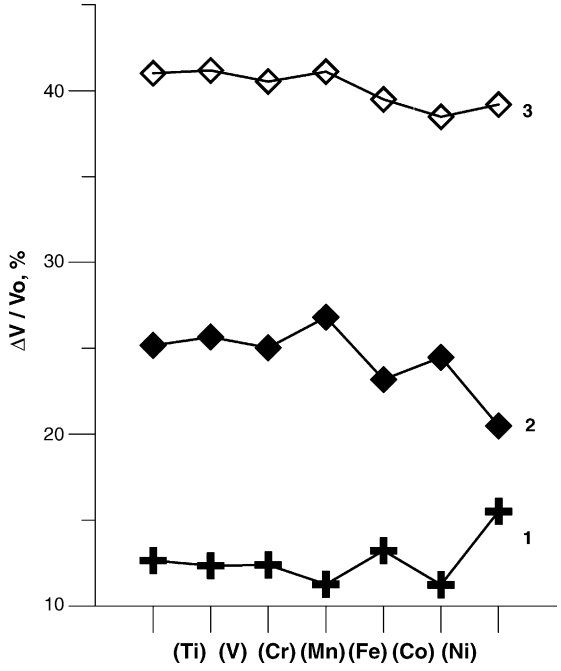

Fig. 2. Relative volume increase per metal atom during the transformations alloy–"monohydride" (1), "monohydride"–"dihydride" (2) and alloy–"dihydride" (3).

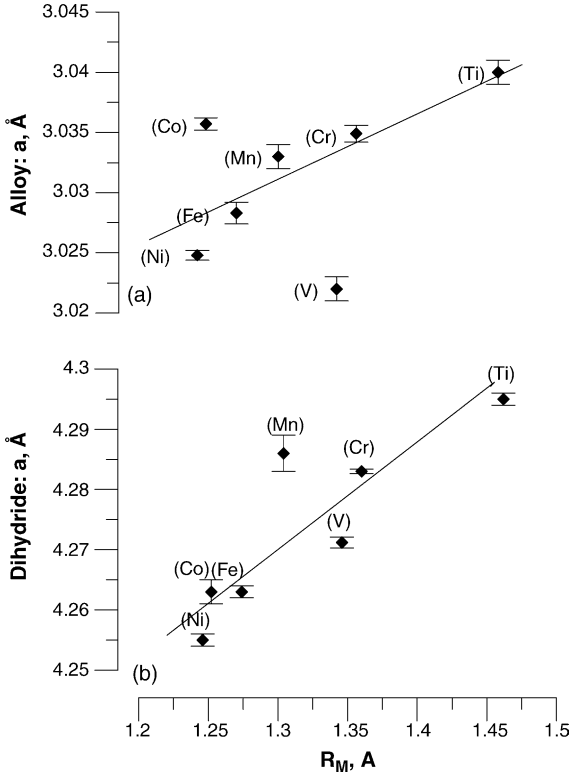

Fig. 3. Correlation between unit cell parameters of the bcc alloys (a) and fcc "dihydrides" (b) and the atomic radii of the substituting elements, M. Lines are drawn just to guide an eye.

trary, the XRD of titanium-contained "monohydrides" were characterised by an increased background and broadened peaks. Apparently, this is caused by high internal stresses in the impact and ductile samples during a transformation of the alloys or "dihydride" phases into tetragonal "monohydrides".

XRD study showed that the formation of the "monohydrides" is accompanied by a volume expansion of 11.3–15.5%. Further hydrogen absorption leads to a more pronounced volume increase, 20.5–26.8% compared to the "monohydride", which in total gives 38.5–41.2% compared to the initial alloys (Fig. 2). The observed values are rather similar for all studied samples and agree well with the reference data: 7.1–12.5 and 24.5–30.7% for "mono-" and "dihydrides", respectively; ~40% in total [12]. Behaviour of the Ni-substituted alloy is very different—it undergoes rather significant expansion (15.5%) during the first step, which markedly reduces volume effect (20.5%) on the step 2. However, the total value (39.2%) is very similar to the other studied alloys.

Interestingly, for the initial alloys and, also for their corresponding dihydrides the parameters of the cubic unit cells systematically increase following a trend in changes of the metallic radii of the elements (see Fig. 3).

3.2. Hydrogen sorption properties

Table 2 summarises hydrogen sorption capacities and activation behaviour of the studied alloys. An overview of the

Table 2
Hydrogen sorption capacities and activation behaviour

Alloy	H sorption capacity				Time of 80% hydrogenation at the first H absorption cycle (min)
	($T = 30\,^{\circ}C$, $P = 25$ bar)		($T < 100\,^{\circ}C$, $P > 0.1$ bar)		
	H/M	cm^3/g	H/M	cm^3/g	
(Ti)	1.76	367.4	0.90	189.3	2.5
(V)	1.65	343.1	0.81	168.2	75
(Cr)	1.79	370.3	1.09	224.7	2.0
(Mn)	1.70	353.2	0.95	197.4	5.5
(Fe)	1.59	328.9	0.76	156.5	12.0
(Co)	1.56	322.7	0.75	155.1	8.5
(Ni)	1.56	321.9	0.88	181.1	16.5

Table 3
PCT properties of the upper plateau segment ($H_{\sim 2} \leftrightarrow H_{\sim 1}$)

Parameter	Alloy						
	(Ti)	(V)	(Cr)	(Mn)	(Fe)	(Co)	(Ni)
Maximum total H capacity (C_{max}), H/M	1.97[a]	1.98	2.02	1.91	1.88	1.77	1.83
	1.99	2.03	2.03		1.85	1.80	1.82
Fraction of the segment in the total capacity	0.47	0.55	0.56	0.53	0.46	0.42	0.48
	0.42	0.52	0.54		0.44	0.41	0.49
H concentration at the plateau midpoint (C_0), H/M	1.30	1.16	1.22	1.20	1.22	1.15	1.13
	1.33	1.24	1.28	1.22	1.19	1.17	1.10
Apparent standard entropy of the transition at C_0 (ΔS^0) (J/mol H_2/K)	−164.63	−146.99	−140.03	−155.64	−153.58	−154.16	−162.89
	−145.11	−153.04	−132.28	−142.67	−127.05	−154.44	−168.17
Apparent standard enthalpy of the transition at C_0 (ΔH^0) (kJ/mol H_2)	−52.98	−40.32	−42.23	−48.10	−43.91	−44.41	−46.04
	−53.36	−44.83	−43.32	−48.45	−40.14	−49.36	−51.35
δ(ln P)/δ(H/M) at C_0 and $T = 60\,^{\circ}C$	3.23	1.11	0.98	3.10	3.08	3.05	2.09
	1.14	0.39	0.31	0.89	1.31	1.50	0.84
$P_{Absorption}/P_{Desorption}$ at C_0 and $T = 60\,^{\circ}C$	12.02	2.46	3.76	5.40	6.25	5.78	3.61

[a] Top—sorption and bottom—desorption.

PCT properties of the hydrides formed by the annealed alloys (derived from the fitting parameters for the upper segments of the PCT curves) is given in Table 3.

Doping by titanium significantly improves the activation properties of the vanadium–zirconium alloy $V_{92.5}Zr_{7.5}$:

(a) Rate of the initial absorption dramatically increases (see Table 2);
(b) Complete reversibility of H desorption is reached in just one cycle compared to the four cycles for $V_{92.5}Zr_{7.5}$;
(c) Both absorption and desorption by the activated alloys become very fast (90% hydrogenation is reached in just 1–4 min compared to 7–8 min for $V_{92.5}Zr_{7.5}$).

An introduction of titanium also increases the total H sorption capacity (except for M = Fe, Co, Ni) and the reversible H sorption capacity (except for M = Fe, Co). The behaviour of the Ni-doped alloy is of special interest: its reversible capacity increases despite a decrease in the total capacity takes place. Such an increase correlates with the observed unusual volume expansion behaviour during the formation of monohydride (Fig. 2). The most pronounced increase both for the total and for the reversible H sorption capacity was observed for M = Cr.

A modification of the alloys with Ti and transition metals (Cr, Mn, Fe, Co, Ni) increases both hysteresis and plateau slope. However, for M = Cr, Ni these parameters decrease approaching the characteristics for the low-alloyed vanadium.

The PCT data show an essential influence of the substituting elements on the thermodynamics of the $VH_{\sim 2} \leftrightarrow VH_{\sim 1}$ transition. At $T = 60\,^{\circ}C$ the equilibrium pressure of hydrogen desorption is around 10 bar for the $V_{92.5}Zr_{7.5}$–H_2 system and close to 0.1 bar for $V_{75}Ti_{17.5}Zr_{7.5}$–H_2. The corresponding values for the quaternary alloys have intermediate values between these limits. This allows, by applying small variations of the amount of the additives of the M-component in V–Zr–Ti–M, to modify hydrogen equilibrium pressure by two orders of magnitude (Fig. 4).

Comparison of the PCT behaviour of the as-cast and annealed alloys showed that, as expected, annealing mainly results in flattening of the plateau area of the desorption isotherms.

The TDS spectra of the hydrogenated samples contain two desorption peaks. The first one appears at low temperatures and corresponds to hydrogen desorption from the "dihydride" ($VH_{\sim 2} \rightarrow VH_{\sim 1}$). The peak position shifts from $-14\,^{\circ}C$ for the least stable hydride on the basis of $V_{92.5}Zr_{7.5}$, to $+10\,^{\circ}C$ for the most stable one formed by $V_{75}Ti_{17.5}Zr_{7.5}$ (Fig. 5a). The observed stability agrees well with corresponding PCT data (Table 3). The second rather broad desorption peak ($VH_{\sim 1} \rightarrow V$) has its maximum at $T \sim 200\,^{\circ}C$ (Fig. 5b).

As it can be seen from Fig. 5b, all titanium-containing samples are characterised by a more broad (compared to $V_{92.5}Zr_{7.5}$) peak of gas evolution, especially for M = Fe, Co, Mn. Introduction of Ti and M reduces the starting temperature for the decomposition of "monohydride" decreasing the thermal stability. In all cases desorption finishes at $T \sim 300\,^{\circ}C$.

4. Applications

Reversible hydrogen sorption capacities of the studied samples are between 155 and 225 cm^3/g (Table 2). They exceed corresponding values for the AB_5 intermetallides and are similar to those for the AB_2 H storage alloys [15]. The possibility to efficiently control the working pressures of the hydrides, by small variations of their chemical composition (Table 3, Fig. 4), makes them promising for the applications in compact, safe and technologically flexible hydrogen storage units and as efficient reversible hydrogen getters for the vacuum plasma technologies [16].

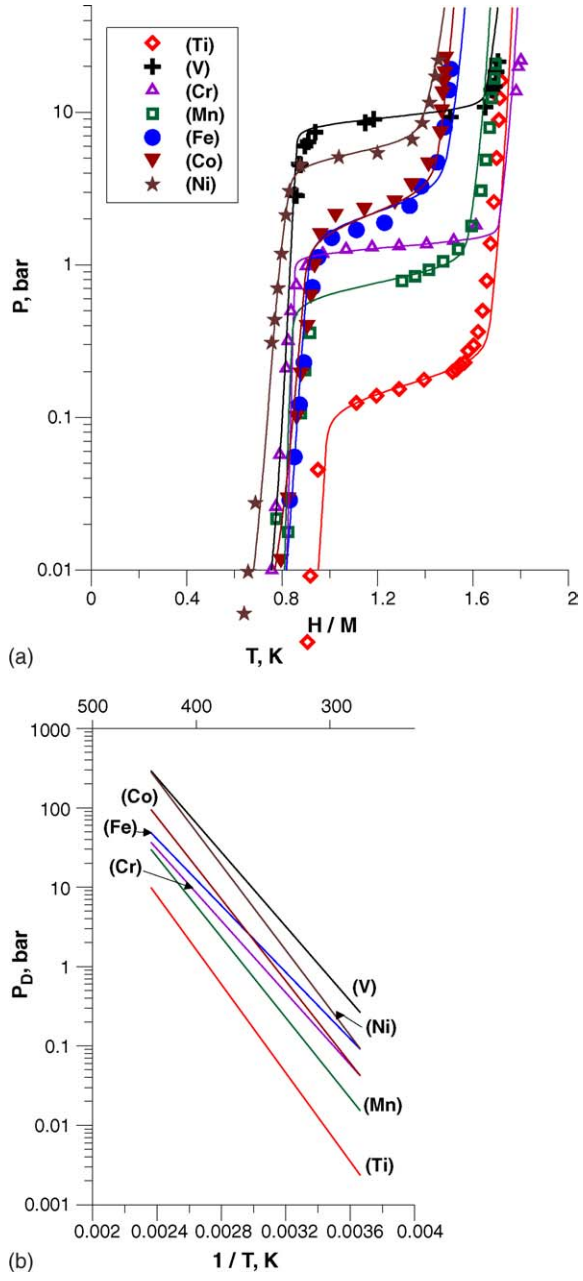

Fig. 4. (a) Hydrogen desorption isotherms at $T = 60\,^{\circ}C$: experimental points and calculated curves; (b) Van't Hoff plots for hydrogen desorption derived from PCT fitting parameters (Table 3).

Especially promising application of the studied V-based alloys is hydrogen thermal sorption compression. From the PCT derived thermodynamic parameters, the use of $V_{92.5}Zr_{7.5}$ and $V_{75}Ti_{10}Zr_{7.5}Ni_{7.5}$ will allow a compression of hydrogen from 20 bar ($T = 10\,^{\circ}C$) to 150–200 bar ($T = 150\,^{\circ}C$) with reversible H capacity exceeding 150 cm^3/g.

Finally, a very efficient separation of hydrogen isotopes can be achieved on the basis of the bcc vanadium alloys. Indeed, as it can be seen from Fig. 6, the alloy $V_{75}Ti_{10}Zr_{7.5}Ni_{7.5}$ shows a strong inverse isotopic effect: at $T = 60\,^{\circ}C$ in the plateau region the pressure ratio P_H/P_D

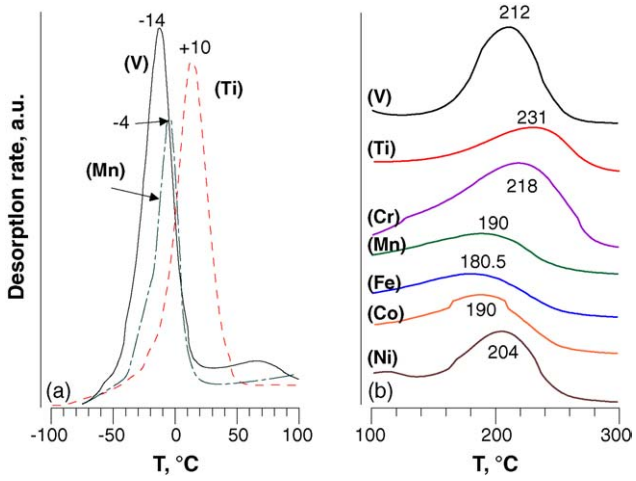

Fig. 5. Hydrogen thermal desorption spectra corresponding to the transitions $VH_{\sim 2} \rightarrow VH_1$ (a) and $VH_{\sim 1} \rightarrow V$ (b).

is close to 2.5. It is higher than isotopic effect recently reported [17] for the $RECo_5$ alloys ($P_D/P_H = 2$). A comparison with the performance of undoped vanadium ([4]; $P_H/P_D \sim 3$ at $T = 40\,^{\circ}C$) reveals two principal advantages of the materials studied in the present work. Firstly, we have not observed a significant difference between absorption–desorption dynamics both for H_2 and D_2, whereas the reaction of D_2 with pure vanadium is much slower compared to hydrogen. Secondly, for the $V_{75}Ti_{10}Zr_{7.5}Ni_{7.5}$ alloy the transition $VH_{\sim 2} \leftrightarrow VH_{\sim 1}$ takes place at the same concentrations both for hydride and deuteride, and maximum sorption capacities are close in both cases. On the contrary, the γ-deuteride on the basis of pure vanadium has much lower reversible sorption capacity than corresponding γ-dihydride [4].

In conclusion, present study shows that vanadium alloys $V_{92.5-x-y}Zr_{7.5}Ti_{7.5+x-y}M_y$ (M = Cr, Mn, Fe, Co, Ni; $x = 0$,

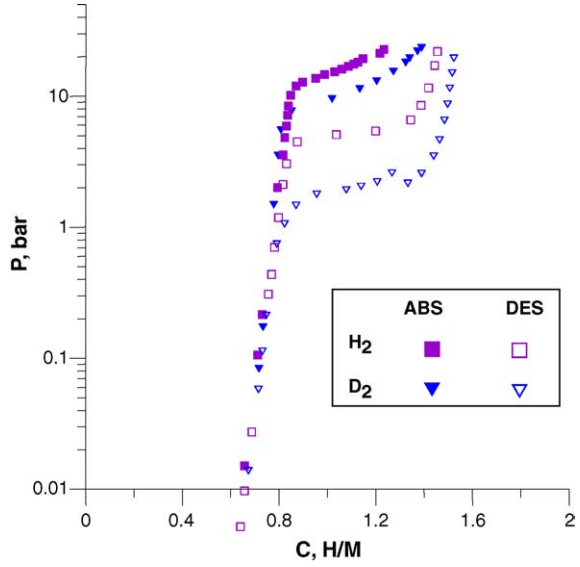

Fig. 6. Isotherms of hydrogen and deuterium absorption and desorption for $V_{75}Ti_{10}Zr_{7.5}Ni_{7.5}$ at $T = 60\,^{\circ}C$.

10; $y = 0$, 7.5) have significant potential for the thermally managed hydrogen storage applications. Possibilities to significantly influence the thermodynamics of the $VH_{\sim 2} \leftrightarrow VH_{\sim 1}$ transition and hydrogen sorption capacity by the substituting M-element are the most valuable features of these systems. Further improvements of the H storage properties can be achieved by reducing the H content in the β-hydride thus increasing the efficient H capacity of the system.

References

[1] W.M. Mueller, J.P. Blackledge, G.G. Libowitz (Eds.), Metal Hydrides, Academic Press, New York–London, 1968, Chapter 12-5.
[2] J.J. Reilly, R.H. Wiswall, Inorg. Chem. 9 (1970) 1678.
[3] G.G. Libowitz, A.J. Maeland, J. Less-Comm. Met. 131 (1987) 275.
[4] R.H. Wiswall, J.J. Reilly, Inorg. Chem. 11 (1972) 1691.
[5] A.J. Maeland, G.G. Libowitz, J.F. Lynch, G. Rak, J. Less-Comm. Met. 104 (1984) 133.
[6] T.B. Flanagan, H. Noh, J.D. Clewley, R.C. Bowman, Scripta Metall. 28 (1993) 355.
[7] A. Kagawa, E. Ono, T. Kusakabe, Y. Sakamoto, J. Less-Comm. Met. 172–174 (1991) 64.
[8] T. Kuriiwa, T. Tamura, T. Amemiya, T. Fuda, A. Kamegawa, H. Takamura, M. Okada, J. Alloys Compd. 293–295 (1999) 433.
[9] E. Akiba, M. Okada, MRS Bull. (2002) 699.
[10] V.V. Burnasheva, V.V. Fokina, V.N. Fokin, S.L. Troitskaya, K.N. Semenenko, Bull. USSR Acad. Sci., Inorg. Mater. 20 (5) (1984) 799.
[11] A. Nowikow, H.G. Baer, Z. Metallk. 49 (1958) 195.
[12] P. Villars, L.D. Calvert, Pearson's Handbook of Crystallographic Data for Intermetallic Phases, 2nd ed., vol. 4, Materials Park, OH 44073.
[13] B.P. Tarasov, J.P. Maehlen, M.V. Lototsky, V.E. Muradyan, V.A. Yartys, J. Alloys Compd. 356–357 (2003) 510.
[14] M.V. Lototsky, V.A. Yartys, V.S. Marinin, N.M. Lototsky, J. Alloys Compd. 356–357 (2003) 27.
[15] G. Sandrock, J. Alloys Compd. 293–295 (1999) 877–888.
[16] M.V. Lototsky, V.A. Yartys, Ye.V. Klochko, V.N. Borisko, R.I. Starovoitov, V.M. Azhazha, P.N. Vyugov, Int. Symp. on Metal–Hydrogen Systems. Fundamentals and Applications (MH–2004). Cracow, Poland, September 5–10, 2004. Abstracts p. 79 (poster Tu–001).
[17] I. Imamoto, S. Mizuaki, Y. Itoh, M. Yamaguchi, 15th World Hydrogen Energy Conference, Yokogama, Japan, June 27–July 2, 2004, 29B–08.